The argon-hydrogen expanding plasma : model and experiments

Plasma Sources Sci. Technol. 4 (1995) 74–85. Printed in the UK

The argon-hydrogen expanding plasma: model and experiments

R F G Meulenbroeks, R A H Engeln, M N A Beurskens, R M J Paffen, M C M van de Sanden, J A M van der Mullen and D C Schram

Eindhoven University of Technology, Department of Physics PO Box 513 5600 MB Eindhoven, The Netherlands

Received 13 July 1994, in final form 26 September 1994

Abstract. An argon expanding cascaded arc plasma, with small amounts (0–10 vol.%) of hydrogen added to the flow, is investigated by means of Thomson–Rayleigh scattering and optical emission spectroscopy. The results, especially the electron density behaviour as a function of the distance from the onset of the expansion, are interpreted by comparison with results of a quasi one-dimensional model. The associative charge exchange reaction between Ar^+ ions and H_2 molecules plays a dominant role in the model. Assuming that H_2 molecules from the wall enter the plasma in the shock region, the large ionization loss can be explained. Good agreement between model and experiment is found for the electron and neutral density and the electron temperature behaviour. This makes plausible the existence of a recirculation flow inside the vacuum vessel, which transports wall-associated hydrogen molecules towards the plasma.

1. Introduction

In a previous paper [1] we reported on the study of a supersonically expanding cascaded arc plasma in argon, with small amounts of hydrogen added to the flow. In the present work we shall extend this study by comparing new measurements to a quasi one-dimensional model. We especially elaborate on the speculation that wall-associated hydrogen molecules play an important role in the large ionization loss in argon plasmas with low hydrogen seed fractions. A re-entry flow of hydrogen molecules into the plasma beam is thought to be caused by wall-associated molecules transported towards the plasma by a strong recirculation flow inside the vessel, as hypothesised by the authors in [1] as well as by De Graaf *et al* [2].

The study of plasmas of this type is important in view of the applications: deposition of thin films and particle sources [2–6].

2. The quasi one-dimensional model

Modelling of a pure argon plasma, expanding out of a cascaded arc source has proved to give good insight into transport phenomena and plasma kinetics [7, 8]. This relatively easy approach will therefore be extended to describe the expansion of an argon–hydrogen plasma. The hydrogen is added to the flow before it enters the cascaded arc. The experiment is shown in figure 1 and has been described in detail elsewhere [1, 3].

2.1. Basic assumptions

Before detailing the equations that govern the expansion, the following basic assumptions will be discussed.

- The plasma is assumed to be ideal, i.e. the velocity distributions for all particles are assumed to be Maxwellian in this type of plasma and the number of electrons within a Debye sphere is assumed to

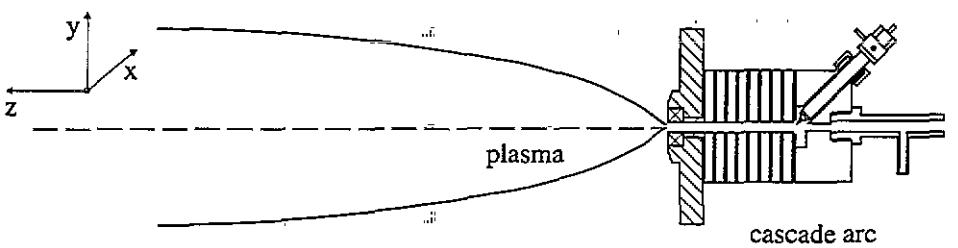

Figure 1. The expanding plasma jet. A subatmospheric plasma (pressure 0.2–0.6 bar) is created inside the cascaded arc, consisting of three cathodes, three electrically isolated copper plates, and an anode plate. The formed plasma expands into a vacuum vessel, creating a supersonically expanding jet.

0963-0252/95/010074 + 12$19.50

be large. The actual minimum value is around 10–20 electrons per Debye sphere.

- The effects of turbulence and viscosity are neglected.
- The assumption is made that hydrogen is totally dissociated for low hydrogen seed fractions (i.e. up to 2 vol.%) in the cascaded arc (T_e, the electron temperature, around 1 eV). Thus, the heavy particles leaving the arc are Ar, Ar^+, H and H^+. Most of the molecular hydrogen in the expanding jet is assumed to originate from the vessel walls [1,2]. The presence of molecular and negative ions (H_2^+, H_3^+, H^-) is neglected. The presence of ArH^+, however, is considered, as this ion is an important intermediate in molecular reactions.
- All heavy particle temperatures are assumed to be equal.
- The charge exchange reaction $Ar^+ + H_2 \rightarrow Ar + H_2^+$ is neglected in favour of the associative charge exchange reaction $Ar^+ + H_2 \rightarrow ArH^+ + H$. This is justified at the temperatures in the expansion which are all well below 0.5 eV [9].
- The energy loss due to line and continuum radiation is neglected compared to other energy losses [3].
- Ohmic dissipation due to pressure induced currents will be neglected despite its known influence on the electron temperature in argon plasma jets [8, 10].
- In the supersonic part of the expansion, axial velocities are assumed to be large compared to the radial velocities.

2.2. The axial velocities of the different particles

One important matter has to be settled: to which extent are the axial velocities of the plasma particles identical when hydrogen as a light 'heavy particle' is added to the plasma? The case of pure argon has been extensively discussed by van de Sanden *et al* [8].

We start by comparing the relaxation times τ_{xy} and mean free paths λ_{xy} for momentum exchange (for particles x in species y) in the expansion as given by [11–13] for the densities close to the stationary shock front and a 2 vol.% H_2 seed fraction: $n_{Ar} = 10^{20}\,m^{-3}$, $n_H \approx n_{H^+} \approx 10^{18}\,m^{-3}$, $n_{Ar^+} \approx n_e \approx 10^{19}\,m^{-3}$. We shall only give the values for the mean free paths, as the relation between τ and λ is well known:

$$\tau_{xy} = \frac{1}{n_y \langle \sigma_{xy} v_{xy} \rangle} \tag{1}$$

and

$$\lambda_{xy} = \frac{v_x}{n_y \langle \sigma_{xy} v_{xy} \rangle} \tag{2}$$

where v_{xy} is the relative speed of the particles, σ_{xy} is the

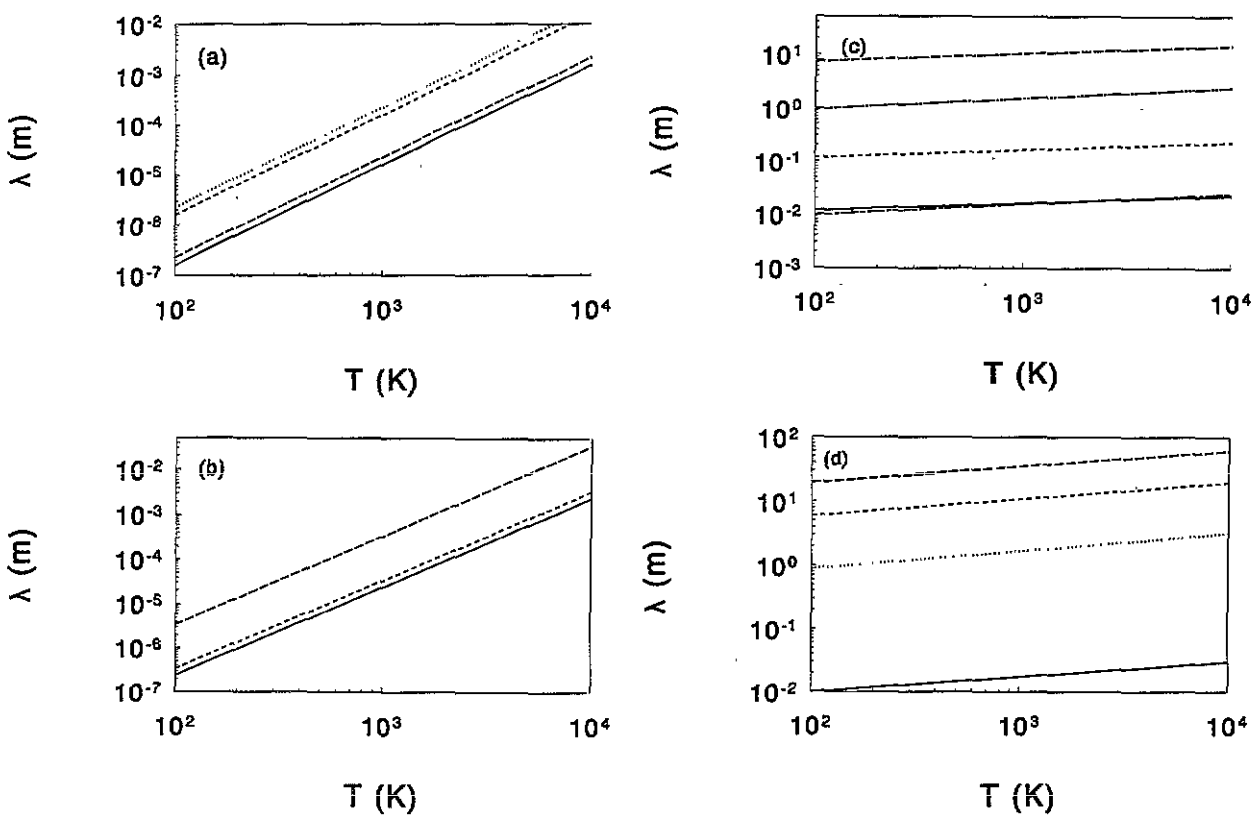

Figure 2. The different mean free paths in the plasma for densities close to the stationary shock front and a 2 vol.% H_2 seed fraction: $n_{Ar} = 10^{20}\,m^{-3}$, $n_H \approx n_{H^+} \approx 10^{18}\,m^{-3}$, $n_{Ar^+} \approx n_e \approx 10^{19}\,m^{-3}$. (*a*) Ion–ion interactions (—, Ar^+–Ar^+; ---, H^+–H^+; – –, H^+–Ar^+; ···, Ar^+–H^+). (*b*) Electron–ion (---, Ar^+–e; – –, H^+–e) and electron–electron (—) interactions. (*c*) Electron–neutral (— – —, e–Ar; — – – —, e–H) and ion–neutral (—, Ar^+–Ar; ---, Ar–Ar^+; – –, H^+–H; ···, H–H^+) interactions. (*d*) Neutral–neutral (—, Ar–Ar; ---, H–H; – –, Ar–H; ···, H–Ar) interactions.

cross section, and τ_{xy} denotes the time constant for momentum exchange from species x to y.

Figure 2 gives the mean free paths for momentum exchange between the different particles. If we examine the mean free paths for the temperature range $T = 2000$–3000 K and compare them to typical gradient lengths in the plasma $L \approx 10^{-2}$–10^{-3} m we can conclude that: (a) all charged particles are coupled; (b) the electron–argon and argon–argon ion mean free paths are small enough; (c) the neutral–neutral coupling could be a problem. Especially the hydrogen atoms appear to be quite free in the argon neutral gas. For the moment, however, we shall assume all axial velocities to be equal to the plasma velocity designated u.

2.3. The system of equations

The expanding plasma can be described by a two gas model—electrons and heavy particles. This method (as well as the quasi one-dimensional approach) is well described by Kroesen *et al* and van de Sanden *et al* [7, 8, 14] and we shall only give a brief outline here.

We start by writing the number balances for the different plasma species. For the electron gas, we neglect two particle recombination, as this process is much less efficient than three-particle recombination under the present conditions [15]. The value of the rate constant for three-particle recombination $K_{\text{rec},3}$ is taken from van de Sanden [15]:

$$K_{\text{rec},3} = 3.3 \times 10^{-21}\, T_e^{-9/2} \tag{3}$$

in units of $\text{m}^6\,\text{s}^{-1}$, with T_e the electron temperature in K. This rate is assumed to be the same for recombination of argon and hydrogen ions, because the recombination of an argon ion usually ends in a highly excited state, where the system is essentially hydrogen-like.

Furthermore, we assume the following associative charge exchange/dissociative recombination reactions to be responsible for ionization loss:

$$\text{Ar}^+ + \text{H}_2 \rightarrow \text{ArH}^+ + \text{H} \tag{4}$$

$$\text{ArH}^+ + \text{e} \rightarrow \text{Ar} + \text{H}^* \tag{5}$$

where the hydrogen molecules are assumed to originate mainly from the vessel walls. An excited hydrogen atom is formed in the second step. For the above reactions, the first step limits the reaction speed, with a rate constant $K_{\text{ArH}^+} = 1.1 \times 10^{-15}\,\text{m}^3\,\text{s}^{-1}$ [16]. This reaction is virtually independent of T_e. The second (dissociative recombination) step is faster by a factor of about 100, depending on n_e.

Thus, we can write the electron number balance as follows:

$$\nabla(n_e \boldsymbol{u}) = -K_{\text{rec},3} n_e^2 (n_{\text{Ar}^+} + n_{\text{H}^+}) - K_{\text{ArH}^+} n_{\text{Ar}^+} n_{\text{H}_2} \tag{6}$$

where n denotes a species density (in m^{-3}) and $\boldsymbol{u}$ is the plasma velocity. The right-hand side of equation (6) will be referred to as B_e from now on.

The number balances for the heavy particles can be written as:

$$\nabla(n_{\text{H}} \boldsymbol{u}) = K_{\text{rec},3} n_e^2 n_{\text{H}^+} + 2K_{\text{ArH}^+} n_{\text{Ar}^+} n_{\text{H}_2} \stackrel{\text{def}}{=} B_{\text{H}} \tag{7}$$

$$\nabla(n_{\text{H}_2} \boldsymbol{u}) = -K_{\text{ArH}^+} n_{\text{Ar}^+} n_{\text{H}_2} + \frac{\phi_{\text{H}_2}}{\pi r^2 l} \stackrel{\text{def}}{=} B_{\text{H}_2} \tag{8}$$

$$\nabla(n_{\text{H}^+} \boldsymbol{u}) = -K_{\text{rec},3} n_e^2 n_{\text{H}^+} \stackrel{\text{def}}{=} B_{\text{H}^+} \tag{9}$$

$$\nabla(n_{\text{Ar}} \boldsymbol{u}) = K_{\text{rec},3} n_e^2 n_{\text{Ar}^+} + K_{\text{ArH}^+} n_{\text{Ar}^+} n_{\text{H}_2} \stackrel{\text{def}}{=} B_{\text{Ar}} \tag{10}$$

$$\nabla(n_{\text{Ar}^+} \boldsymbol{u}) = -K_{\text{rec},3} n_e^2 n_{\text{Ar}^+} - K_{\text{ArH}^+} n_{\text{Ar}^+} n_{\text{H}_2} \stackrel{\text{def}}{=} B_{\text{Ar}^+} \tag{11}$$

where B_{H}, etc are short-hand notations for the respective right-hand sides (RHSs). In the calculations an extra input is added to B_{H_2} (second term RHS in (8)) in order to simulate a re-entry flow of wall associated hydrogen molecules to the plasma beam. In equation (8), ϕ_{H_2} denotes the total radial influx (in s^{-1}), r denotes the plasma radius, and l represents the length of the absorbing part of the beam, i.e. the distance over which H_2 molecules enter the plasma. This distance does not include the length of the shock region, which is treated separately and analytically (see next section).

The total balance for the mass density ρ reads:

$$\nabla(\rho \boldsymbol{u}) = 0. \tag{12}$$

The equation for the total momentum balance (without viscosity and the Lorentz force) is written as:

$$\rho(\boldsymbol{u} \cdot \nabla) \cdot \boldsymbol{u} + \nabla p = 0 \tag{13}$$

where $p = k(n_e T_e + n_h T_h)$ is the total pressure. T_h is the heavy particle temperature and k is Boltzmann's constant. In principle $\rho = \Sigma_x m_x n_x$ includes all plasma species x with masses m_x. In our case with small hydrogen seed fractions (<2%), however, we can simplify this expression using the fact that electrons, H^+, H, and H_2 particles are all much lighter than argon atoms or ions. With a very small error (<0.1%) we can therefore simply write:

$$\rho \approx m_{\text{Ar}}(n_{\text{Ar}} + n_{\text{Ar}^+}) = m_{\text{Ar}}(n_{\text{Ar}} + n_e). \tag{14}$$

Finally, we need the two energy balances for the electrons and the heavy particles (without viscosity term):

$$\nabla \cdot (\tfrac{3}{2} n_h k T_h \boldsymbol{u}) + n_h k T_h (\nabla \cdot \boldsymbol{u}) + \nabla \cdot \boldsymbol{q}_h = Q_h \tag{15}$$

$$\nabla \cdot (\tfrac{3}{2} n_e k T_e \boldsymbol{u}) + n_e k T_e (\nabla \cdot \boldsymbol{u}) + \nabla \cdot \boldsymbol{q}_e = Q_e \tag{16}$$

with $\boldsymbol{q}_x$ the particle heat flux ($\boldsymbol{q}_x = -\kappa_x \nabla T_x$, with κ_x the thermal conductivity for species x and T_x the corresponding temperature) and $Q_{h,e}$ the energy source terms for the respective particles. The particle heat flux is taken into consideration in a simplified form, following van de Sanden *et al* [8]: only the radial heat flux is considered, as a loss term. With argon as the dominant species, the heavy particle energy source term can be written as:

$$Q_h = Q_{eh} + Q_{\text{diss.rec.}} - Q_q \tag{17}$$

with:

$$Q_{eh} = 3\frac{m_e}{m_{Ar}} n_e \left(\frac{1}{\tau_{e,Ar^+}} + \frac{1}{\tau_{e,Ar}}\right) k(T_e - T_h) \quad (18)$$

$$Q_{diss.rec.} = K_{ArH^+} n_{Ar^+} n_{H_2} \tfrac{3}{2} k T_e \quad (19)$$

$$Q_q = \frac{\kappa_h T_h}{r^2} \quad (20)$$

where Q_q represents the radial heat conduction in a simplifed form, as an energy loss term: κ_h is taken from Braginskii [11] and r denotes the plasma radius. This is a simplified form valid if the temperature profile is taken to be a Gaussian [8]. The values for the relaxation times for momentum transfer τ_{e,Ar^+} and $\tau_{e,Ar}$ are taken from the works of Braginskii [11] and Timmermans [13]. For the energy transfer between electrons and heavy particles due to reactions (4) and (5) we assume that a *thermal* electron is lost, i.e. the electron temperature is not very much affected. This is justified by the fact that the temperature dependence of K_{ArH^+} is not very strong in the temperature range considered here [16]. The heavy particle, however, gains the energy of the lost electron, which equals $\frac{3}{2}kT_e$. The heavy particles could gain more from the dissociative recombination, but this is not taken into account.

The electron energy source term can be written as:

$$Q_e = Q_{rec,3} - Q_{eh} - Q_q \quad (21)$$

with the three-particle recombination source term:

$$Q_{rec,3} = K_{rec,3} n_e^2 (n_{Ar^+} \Delta E_{Ar} + n_{H^+} \Delta E_H) \quad (22)$$

and the 'loss' by heat conduction:

$$Q_q = \frac{\kappa_e T_e}{r^2}. \quad (23)$$

The amount of energy gained by the second electron in the reaction $A^+ + e + e \rightarrow A^* + e$ is approximately equal to 0.15 times the ionization energy of the species concerned, depending on n_e (van de Sanden *et al* [15]). This determines the values of ΔE_H and ΔE_{Ar} in equation (22).

It is convenient to introduce dimensionless parameters α, β, δ and ε instead of the particle densities:

$$n_e = \frac{\alpha\rho}{m_{Ar}} \quad (24)$$

$$n_{H_2} = \frac{\beta\rho}{m_{Ar}} \quad (25)$$

$$n_H = \frac{\delta\rho}{m_{Ar}} \quad (26)$$

$$n_{H^+} = \frac{\varepsilon\rho}{m_{Ar}}. \quad (27)$$

The equations discussed so far can be rewritten to form a system of eight first-order differential equations with eight variables: α, β, δ, ε, T_e, T_h, ρ and u [7, 10], where u is a scalar: the axial expansion speed.

We can now combine the above equations to a complete set:

$$\frac{du}{dz} = -\frac{u}{(1-M^2)}\left(\frac{1}{A}\frac{dA}{dz}\right) + \frac{2}{5}\frac{Q_e + Q_h}{\mathscr{R}\rho T_p(1-M^2)} \quad (28)$$

$$\frac{d\rho}{dz} = \frac{\rho M^2}{(1-M^2)}\left(\frac{1}{A}\frac{dA}{dz}\right) - \frac{2}{5}\frac{Q_e + Q_h}{\mathscr{R}\rho T_p(1-M^2)} \quad (29)$$

$$\frac{dT_h}{dz} = \frac{2}{3}\frac{T_h M^2}{(1-M^2)}\left(\frac{1}{A}\frac{dA}{dz}\right) + \frac{2}{3}\frac{Q_h}{\rho u \mathscr{R}} - \frac{4}{15}\frac{T_h}{T_p}\frac{Q_e + Q_h}{\mathscr{R}\rho u(1-M^2)} \quad (30)$$

$$\frac{dT_e}{dz} = \frac{2}{3}\frac{T_e M^2}{(1-M^2)}\left(\frac{1}{A}\frac{dA}{dz}\right) + \frac{2}{3}\frac{Q_e}{\alpha\rho u\mathscr{R}} - \frac{4}{15}\frac{T_e}{T_p}\frac{Q_e + Q_h}{\mathscr{R}\rho u(1-M^2)} - \frac{m_{Ar}T_e B_e}{\alpha\rho u} \quad (31)$$

$$\frac{d\alpha}{dz} = \frac{m_{Ar}B_e}{\rho u} \quad (32)$$

$$\frac{d\beta}{dz} = \frac{m_{Ar}B_{H_2}}{\rho u} \quad (33)$$

$$\frac{d\delta}{dz} = \frac{m_{Ar}B_H}{\rho u} \quad (34)$$

$$\frac{d\varepsilon}{dz} = \frac{m_{Ar}B_{H^+}}{\rho u}. \quad (35)$$

Equation (28) is obtained by combining the momentum and energy balances ((13), (15), and (16)); equation (29) by using (28) and the mass balance (12); equations (32)–(35) by using the mass balances (12) and (6)–(9). Finally, equations (30)–(31) are derived using (28), (29) and (32).

In the above equation set, M denotes the plasma Mach number, defined by:

$$M^2 = \frac{3u^2 m_{Ar}}{5kT_p} \quad (36)$$

with $T_p = T_h + \alpha T_e$ the plasma temperature. The gas constant $\mathscr{R}$ is given by:

$$\mathscr{R} = \frac{k}{m_{Ar}}. \quad (37)$$

Note, that in equations (36) and (37) argon is assumed to be the main species. In the quasi one-dimensional case, A corresponds to the surface over which the plasma parameters are averaged to make the problem one dimensional. For A, the following equation:

$$\frac{1}{A}\frac{dA}{dz} = \frac{2\tan\phi}{r} \quad (38)$$

holds, where ϕ is half the angle of expansion and r is the radius of the plasma at a certain axial position z [7].

It may be noted that the equation set (28)–(35) basically represents the pure argon model as treated by van de Sanden *et al* [8] with a perturbation due to the presence of hydrogen. The gas dynamical behaviour of

the plasma is equal to the pure argon case (we shall return to this later when we discuss the neutral particle density measurements). The hydrogen, however, appears to play a decisive role in the plasma kinetics. This will become clear when the electron density behaviour is discussed. This approach with hydrogen as a perturbation is allowed for low hydrogen seed fractions, as the masses of all hydrogen atoms, molecules, and ions are all much lower than the masses of the argon atoms and ions.

Equations (28)–(35) form a complete set and will be solved numerically by Runge–Kutta integration to cover the first (supersonic) part of the expansion. The stationary shock front will be treated analytically in the next section.

2.4. The stationary shock front

To describe a discontinuity in flow variables, one could in principle use the Rankine–Hugoniot relations, as was done by Kroesen *et al* [7]. A better approximation is obtained with the method developed by Mott–Smith [8, 10, 17–19]. In order to get an impression of the shape of the shock, we assume the shock to be identical for all particles. In the shock region ($z = 40$–70 mm) the numerical integration is taken over by an analytical approach, in which T_h, u and ρ are transformed according to the Mott-Smith relations (for a ratio of specific heats $\gamma = 5/3$):

$$\frac{\rho(z)}{\rho(0)} = \frac{4M_0^2 + (M_0^2 + 3)\exp[-4(z - z_0)/L_0]}{(M_0^2 + 3)\{1 + \exp[-4(z - z_0)/L_0]\}} \quad (39)$$

$$\frac{u(z)}{u(0)} = \frac{\rho(0)}{\rho(z)} \quad (40)$$

$$\frac{T_h(z)}{T_h(0)} = \frac{1}{4}\left[\frac{14}{5}\left(\frac{\rho(0)}{\rho(z)} - \frac{1}{4}\right)^{-1} - 1\right]\frac{\rho(0)}{\rho(z)}. \quad (41)$$

In the above set of equations, L_0 represents the shock thickness. In our first approximation λ_{00}, the neutral particle mean free path (argon in argon), is taken as a measure for L_0. Following van de Sanden *et al* [8], we take $L_0 \approx 4\lambda_{00}$ for high Mach numbers M_0 (around ten) before the shock. The Mott–Smith relations are taken relative to the center of the shock region: z_0 denotes the middle of the shock region. $\rho(0)$, $u(0)$, and $T_h(0)$ denote the values of the flow variables before the shock.

In the shock, all densities are transformed like the mass density ρ. The H_2 density, however, can be changed at each position to account for a re-entry flow of hydrogen molecules into the jet. This extra input of hydrogen molecules constitutes the major fitting parameter when comparing the model to the experiments, as the existence of a re-entry flow has only been hypothesised so far.

The electrons themselves do not experience a shock, since their motion never becomes supersonic (because of their low mass, equation (36)): it is the ion shock that dictates the electron density in the shock region (quasi-neutrality). As a consequence, the electron temperature is not transformed in a way similar to the heavy particle temperature. Adiabatic compression is assumed in order to calculate the electron temperature at each axial position in the shock. For a ratio of specific heats $\gamma = 5/3$, this relation reads:

$$\frac{T_e(z)}{T_e(0)} = \left(\frac{n_e(z)}{n_e(0)}\right)^{2/3}. \quad (42)$$

The actual position of the shock front is obtained by equating the stagnation pressure p_{stag} to the vessel background pressure p_{back} at each point in the expansion. When the former exceeds the latter, the shock position z_{shock} is found. The program then uses equations (39)–(42) to calculate ρ, u, T_h and T_e for the range $(z_{shock} - L_0)$ to z_{shock}. The middle of the shock region (z_0) is situated at $z_{shock} - \frac{1}{2}L_0$. After the shock (in the subsonic region) numerical integration starts again, using the values obtained from the analytical expressions as starting values. The analytical shock calculation causes a small discontinuity in the calculated profiles around $z_{shock} - L_0$.

2.5. The subsonic relaxation region

In the region after the shock, axial gradients are no longer large compared to the radial gradients. This means, that the radial expansion of the beam is mainly diffusion determined [7]. The model uses equations (28)–(35) again to calculate the values of the parameter set. The difference with the supersonic expansion part is, that the angle of expansion ϕ is now given by:

$$\tan\phi = \mathscr{F}\frac{D}{ru} \quad (43)$$

where r is the plasma radius, $\mathscr{F}$ is a constant depending on the actual shape of the plasma radial profile, and D is a diffusion coefficient. The value of $\mathscr{F}$ is around two for any reasonable plasma profile (e.g. a Gaussian or a parabolic) [7]. D is assumed to be equal to the ambipolar diffusion coefficient for a pure argon plasma [7, 13]:

$$D = \frac{5.52 \times 10^{18}}{n_0 + n_e} T_e T_i^{-0.36}. \quad (44)$$

When applying equation (44), $T_i \approx T_h$ is assumed; n_0 denotes the neutral particle density.

This concludes the discussion of the model.

3. Experiments

3.1. Thomson–Rayleigh scattering measurements

3.1.1. Axial scans. As in the previous paper [1], the expanding argon–hydrogen plasma jet is investigated both by active and passive spectroscopic means. The Thomson–Rayleigh diagnostic has been described extensively by van de Sanden [3] and we will not repeat the description here. In short, frequency doubled

Nd:YAG radiation is focused into the plasma and the scattered photons (under a 90° angle) are dispersed by a polychromator and detected by an image intensified photo diode array. The only difference from the previous set-up [1] is the fact that the Nd:YAG laser has been replaced by a more powerful type (Quanta Ray GCR-190, 250 mJ per pulse at 532 nm, 50 Hz). This results in shorter measurement times.

The parameters, determined by Thomson–Rayleigh scattering are n_e, T_e and n_0, with accuracies of about 10%, 25%, and 15% respectively. Due to the small Rayleigh scattering cross sections for H and H_2 and the small densities of these species compared to the argon neutral density, the measured neutral densities are equal to the argon neutral densities. The parameters are determined locally (detection volume about 0.25 mm^3). The measurements are performed on the plasma in figure 1 under the following conditions: arc current $I_{arc} = 45$ A, arc voltage $V_{arc} = 100$ V, background pressure $p_{back} = 40$ Pa, total flow (argon and hydrogen): 3.5 standard litres per minute, hydrogen flow 0–10 vol.%. The hydrogen is admixed to the argon before it enters the cascaded arc. For seed fractions of 0, 2, 3, 4, 5, and 10 vol.%, axial scans are performed. Radial scans are performed for 0 and 2 vol.% seed fractions. As the cascaded arc can be moved inside the vessel without significantly changing the plasma, axial and radial scans can be made with great ease—without moving the laser system.

The experiments for a 'pure' argon plasma (i.e. with the possible pollution of hydrogen molecules originating from the vessel walls [1,2]) and for a 2 vol.% hydrogen seed fraction are compared to the model. The reason for leaving out the higher percentages lies in the fact that the behaviour of the arc itself changes severely when more than, say, 3 vol.% hydrogen is admixed. This is reflected in the fact that with a 5 or 10 vol.% seed fraction, the electron density just after the arc exit drops to very low values (a few times 10^{18} m^{-3}).

In figure 3, the axial electron density profiles are presented. The observed agreement between model and experiments is very good. In the case of 2 vol.% hydrogen, a total H_2 inflow from the vessel walls into the plasma of about 4×10^{18} particles per second is implemented in the model. The extra input has to take place before and in the shock region, i.e. between $z = 0$ and $z = 70$ mm. The input is assumed to be constant over this region. If an input in the subsonic region is assumed, the agreement between model and experiments is significantly poorer. This is in agreement with our earlier hypothesis [1]. The value of 4×10^{18} s^{-1} depends largely on the re-entrance flow pattern. In our case, where a constant radial inflow is assumed, the actual value is very sensitive to changes in the magnitude of the external hydrogen input. The total flux of re-entering hydrogen molecules has to be compared to the total quantity of molecules entering the arc: 2 vol.% hydrogen corresponds to approximately 2.5×10^{19} s^{-1}.

As for the 'pure' argon case, we still had to assume a 2.4×10^{17} s^{-1} re-entry flow. This is to be expected, as the saturation of the vessel walls with hydrogen during

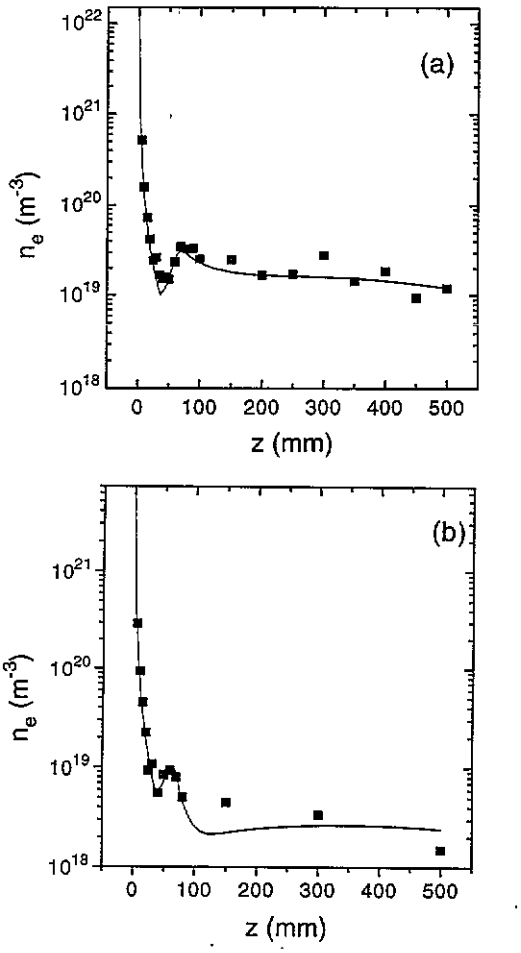

Figure 3. The electron density against the axial position (distance from the onset of the expansion). (*a*) For a pure argon flow entering the arc and (*b*) for a 2 vol.% hydrogen admixture. The drawn lines present the results of the model as described in the main text.

hydrogen experiments will still cause a (smaller) re-entry flow of hydrogen molecules when returning to a pure argon plasma. The emission spectroscopy work (to be discussed later) confirms this as the hydrogen Balmer series are still observed when the arc is burning on pure argon. Also in this case, the model is very sensitive to the magnitude of the re-entry flow. The extra input has to take place before and in the shock: addition of extra hydrogen in the subsonic region causes the model values to deviate strongly after $z = 100$ mm. It should be stressed that an external input of hydrogen molecules is absolutely necessary to obtain a good agreement between model and experiments.

The axial scans for higher admixtures of hydrogen (figure 4) are not compared to the model because it is almost certain that the behaviour of the arc itself changes severely when, e.g. 10 vol.% H_2 is added. This aspect needs further research. For a 10 vol.% seed fraction, the ion flux from the arc has decreased significantly, as the electron density at $z = 5$ mm has dropped to a low value (around 10^{18} m^{-3}, compare figure 3).

Figure 5 gives the neutral densities versus the axial position. Here also, the model describes the experiments very well. The neutral density behaviour appears to be

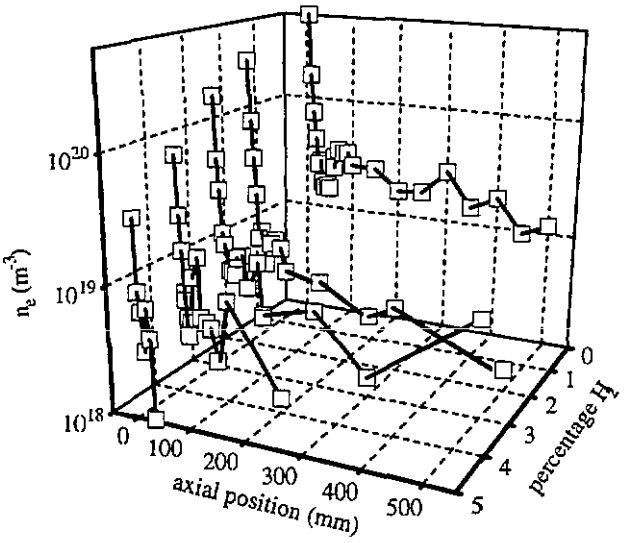

Figure 4. The electron density against the axial position (z) for higher admixtures.

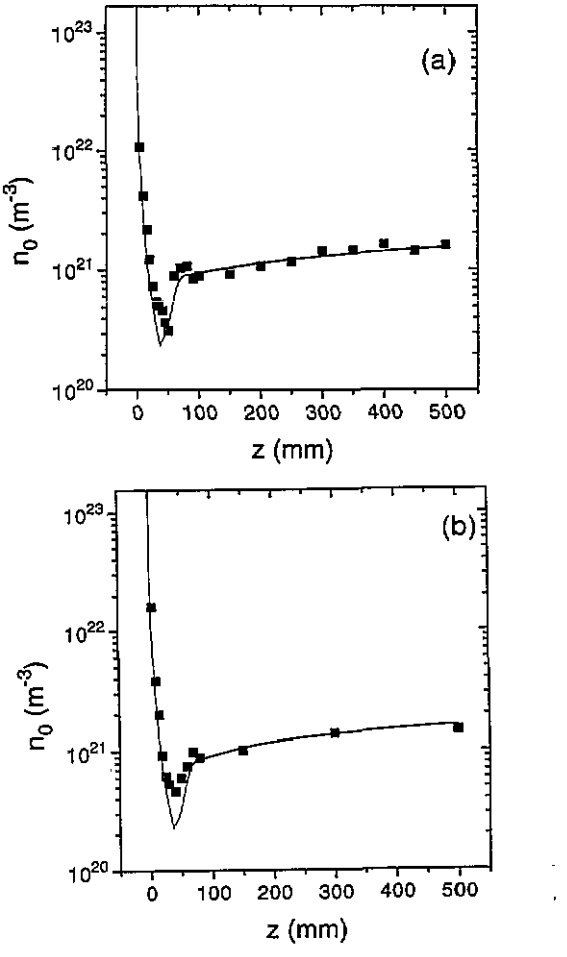

Figure 5. The neutral density against the axial position z for (*a*) pure argon and (*b*) a 2 vol.% hydrogen admixture. The drawn lines present the results of the model.

independent of hydrogen seed fraction. So our initial assumption [1] that we could study the plasma beam kinetics without disturbing the basic transport phenomena remains justified (at least up to 5 vol.% H_2 seed fractions). So, as was mentioned before, we can consider

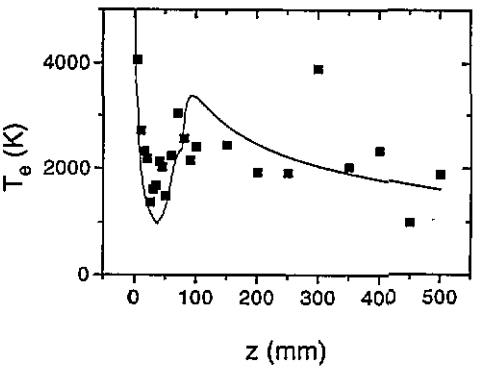

Figure 6. The electron temperature against the axial position z for pure argon. The drawn line represents the model. The 2 vol.% data show too much scatter to make a comparison with the model useful.

hydrogen to be a small perturbation on the argon expanding jet, as far as transport phenomena are concerned.

The electron temperature behaviour is difficult to describe, as was pointed out by van de Sanden [8]. Especially in the shock region, current generation appears to be of importance, causing the electron temperature to rise before the actual shock position. As our model does not include current generation, the agreement between model and experiments is not expected to be very good. Nevertheless, the general trends are clear in figure 6. The data for hydrogen admixture show too much scatter to make a useful comparison with the model. Further research is needed to get more insight into the electron temperature behaviour when hydrogen is admixed to the flow.

3.1.2. Radial scans. For 0 and 2 vol.% hydrogen seed fractions, radial scans have been performed at five axial positions: $z = 10$, 20, 40, 70 and 100 mm. The results for the electron density and temperature as well as the neutral density are given in figure 7 and 8. In particular, the electron density profiles support the view that hydrogen molecules enter the plasma beam from the periphery. This becomes clear in figure 9. Here, we have used the adiabatic model by Ashkenas and Sherman [20] to fit the radial profiles at $z = 10$ and 20 mm. For the 'pure' argon case, the fits appear to be quite good, especially at $z = 10$. This is an extra confirmation of the view [3] that the supersonic part of the pure argon jet closely resembles an adiabatic expansion.

For the 2 vol.% case, we simply used the fits for the pure argon case and normalized them to the maximum value (at $r = 0$ mm) of the 2 vol.% radial scans. The results are also shown in figure 9. It can clearly be seen that the adiabatic expansion model no longer coincides with the measurements: the measurements tend to be much lower than they would have been in the case of an adiabatic expansion. The simple transfer of the pure argon fits to the 2 vol.% data is justified, because the adiabatic model only depends on the specific size and form of the expansion hole and the pressure ratio inside and outside the expansion chamber [20]. In our view,

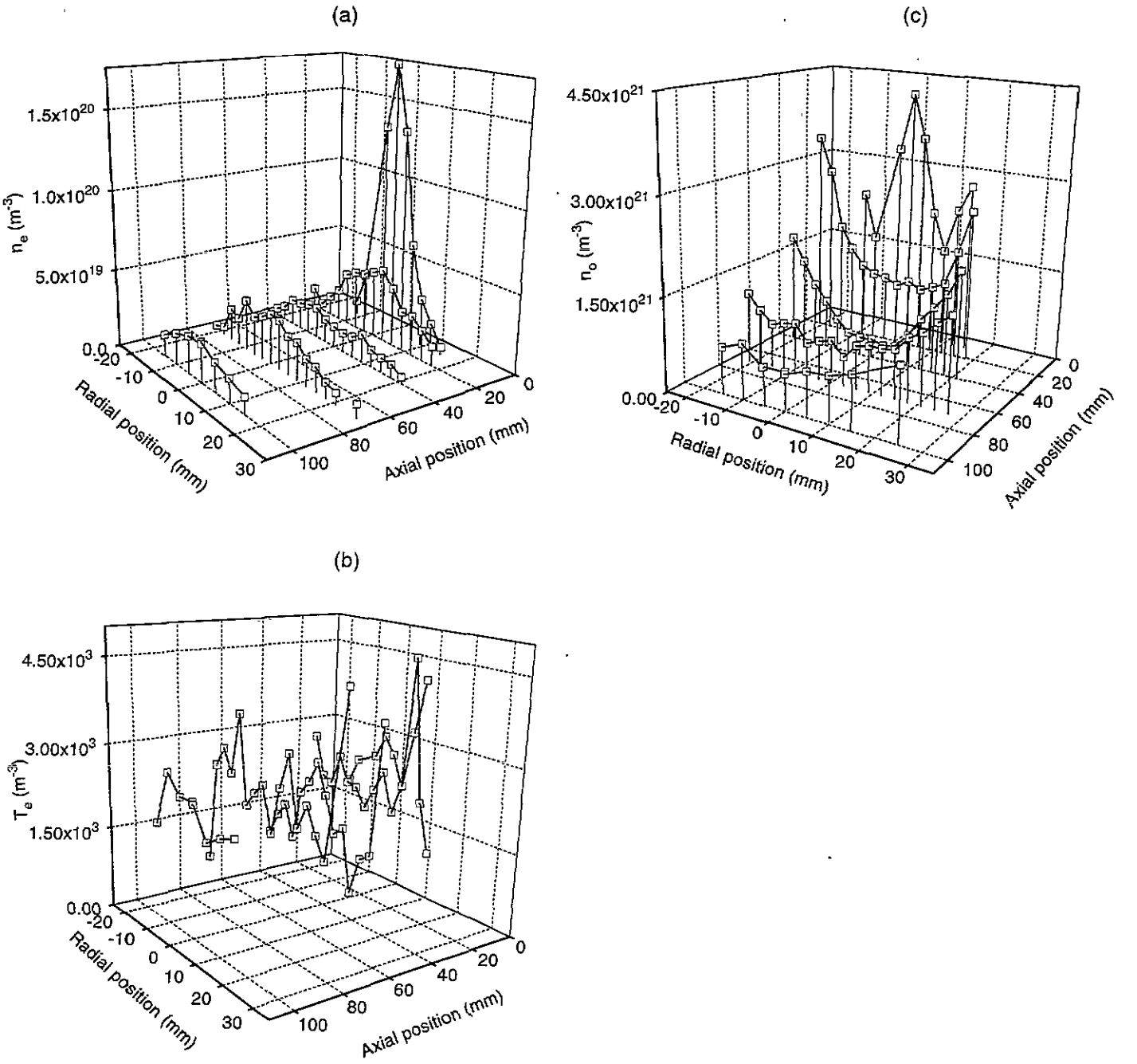

Figure 7. Radial profiles for the electron density n_e (*a*), the electron temperature T_e (*b*), and the neutral density n_0 (*c*): pure argon.

this is a clear hint that reactions (4) and (5) take place at the edges of the plasma, and that a radial re-entry flow of hydrogen molecules is needed to make this possible. The effect on the central electron density could have two reasons: arc effects or the occurrence of the same reactions. This latter process is not expected to have much influence, however, before $z = 30$–40 mm.

3.2. Optical emission spectroscopy

Even though line and continuum radiation are not taken into account in the discussed model, optical emission spectroscopy (OES) results can give extra insight in the plasma beam kinetics. The OES measurements have proved to be especially effective in combination with the Thomson–Rayleigh scattering results. The OES diagnostic has been extensively discussed elsewhere [1, 10] and we will only give the results here.

OES measurements have been performed on the same set of Ar(I) and H(I) lines as reported in our previous paper [1], at three axial positions: $z = 20$, 40 and 70 mm and for the same hydrogen seed fractions as mentioned above. The OES system was calibrated using a tungsten ribbon lamp in order to obtain absolute level densities per statistical weight. We choose to present the data in the form of population factors b_p. In this representation, the absolute level density per statistical weight (n_p/g_p) is related to the density as calculated with the Saha equa-

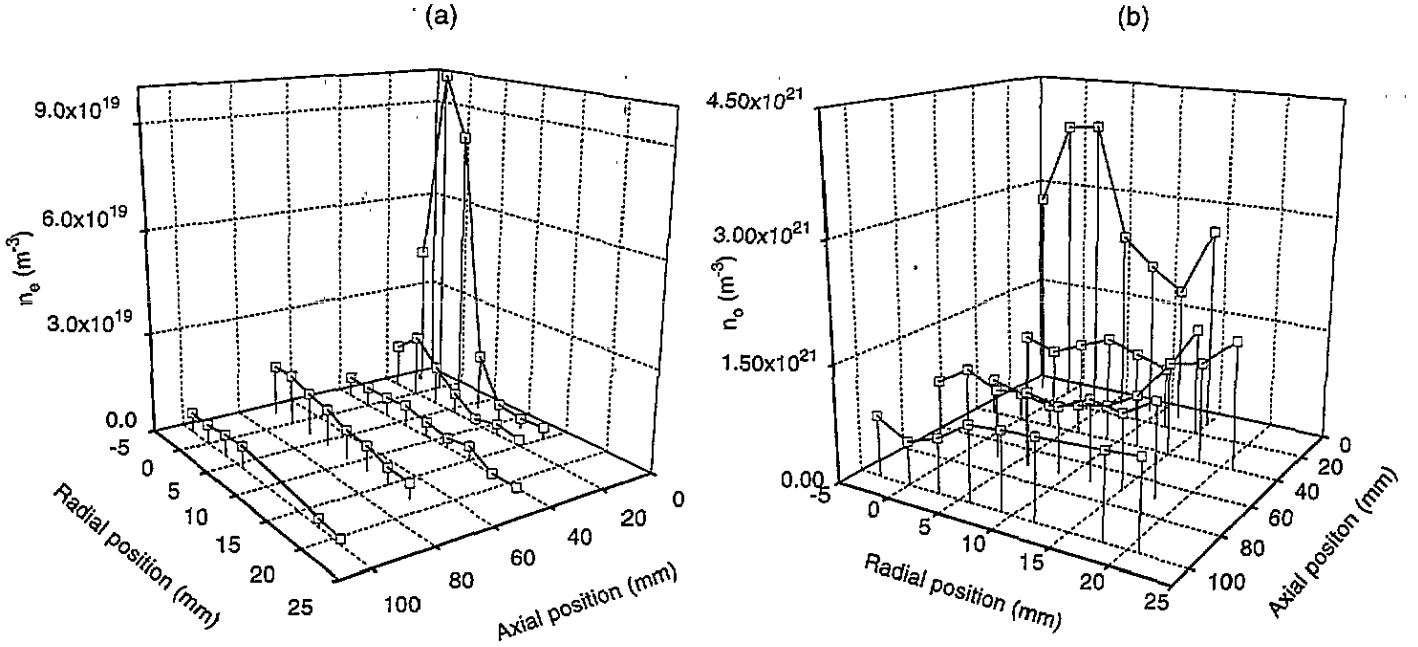

Figure 8. Radial profiles for the electron density n_e (*a*) and the neutral density n_0 (*b*) for a 2 vol.% hydrogen admixture.

tion ($n_{p,Saha}/g_p$) [1, 21]:

$$b_p \stackrel{def}{=} \frac{n_p}{n_{p,Saha}} \quad (45)$$

where the Saha density $n_{p,Saha}$ is calculated using the n_e and T_e values obtained by Thomson scattering. To calculate the H Saha density, we need the H^+ density. The latter is calculated using intensity ratios of highly excited hydrogen and argon levels, as was discussed previously [1].

In general, a strong decrease in intensity of the argon lines is observed if hydrogen is admixed, as reported before. As the excitation in the argon system results from three-particle recombination [15], this must be a consequence of the disappearance of argon ions. Two processes can be responsible for this loss: (a) the occurrence of reactions (4) and (5), and (b) the arc ionization changing from argon to hydrogen, as the ionization potential of hydrogen is smaller by about two eV [1]. For seed fractions above 4 vol.% hydrogen, even the strongest argon lines disappear.

The behaviour of the hydrogen line intensities is more complicated. The intensity rises with the hydrogen admixture until 3 vol.%, after which it drops (figure 10). The effect can be explained by assuming that the excitation in the hydrogen system is a result not only of three-particle recombination, but also of the occurrence of reactions (4) and (5). We assume for the moment that the total arc ionization degree remains more or less constant until 3 vol.% hydrogen is admixed, above which the ionization degree must drop dramatically to explain the low n_e value measured by Thomson scattering. The increase in hydrogen line intensities can, then, be explained by: (a) the fact that more and more hydrogen molecules enter the plasma beam to participate in reaction (4); and (b) the fact that more and more hydrogen ions are coming out of the arc. The former effect could, however, be balanced by the decrease in the amount of argon ions leaving the arc. The decrease for higher seed fractions (>3 vol.%) must be a consequence of the arc becoming less efficient in producing (predominantly hydrogen) ions—as indicated by the Thomson scattering data.

It was also observed that the hydrogen Hα line is clearly visible when *no* hydrogen is added to the flow. This was observed by Meeusen *et al* in a similar situation [23]. The Hα emission appeared to decrease slowly (on an hour time scale). In our view, this can only be explained by a recirculation flow inside the vessel in combination with a stainless steel vessel wall saturated with hydrogen [1].

The population factors for the argon and hydrogen systems are depicted in figure 11. The general shape of the Ar(I) and H(I) distributions is similar to those reported before [1], so only one example is given. As can be seen, the Ar(I) b_p factors close to the continuum approach the value 1, indicating the presence of a Saha equilibrium, as expected for this type of recombining plasma. This constitutes a test for both the Thomson data and the OES calibration [1, 21].

More remarkable is the 'bulge' in the hydrogen b_p factors around p (principal quantum number) = 5–7. It has been verified, that this effect cannot be attributed to Stark broadening, an effect which could boost the width of the hydrogen Balmer lines above the width of the apparatus profile of the monochromator, thus causing a systematical error (as higher excited levels are Stark broadened more strongly). This can be thoroughly tested by recording wavelength scans of the different Balmer lines: for all lines, the line profile appears to be equal to the monochromator apparatus profile. If Stark

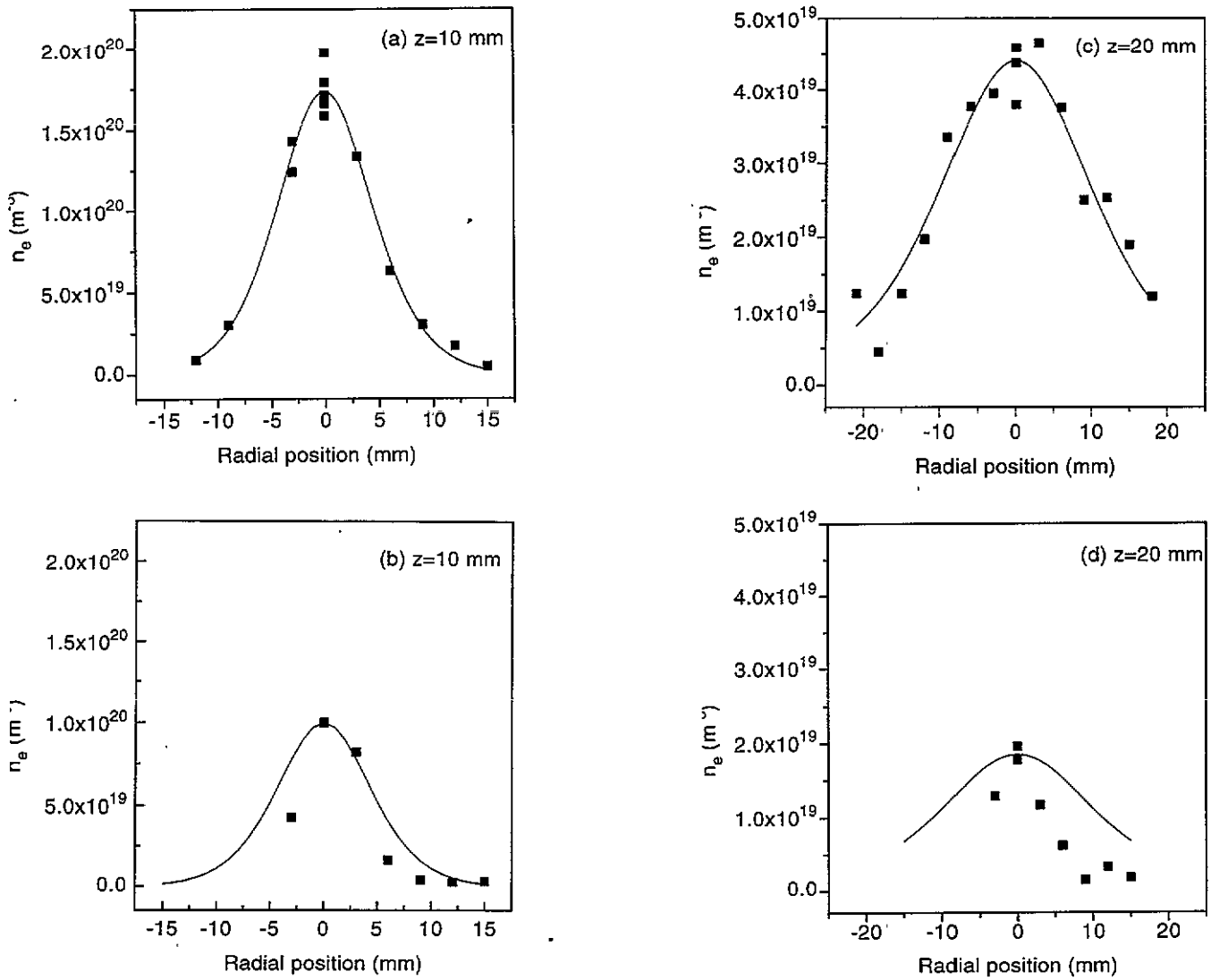

Figure 9. Radial scans for $z = 10$ mm ((*a*) pure argon, (*b*) 2 vol.% hydrogen) and $z = 20$ mm ((*c*) pure argon, (*d*) 2 vol. % hydrogen). The drawn lines represent the Ashkenas and Sherman [20] adiabatic model for a supersonically expanding jet. The 2 vol. % data cannot be described with the adiabatic model.

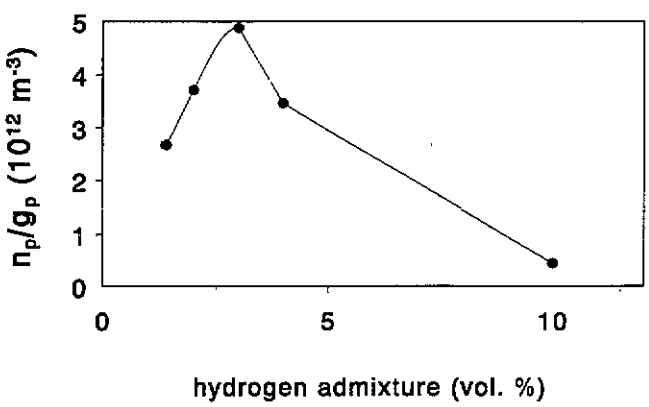

Figure 10. The hydrogen $p = 5$ level population per statistical weight against the hydrogen seed fraction at $z = 20$ mm.

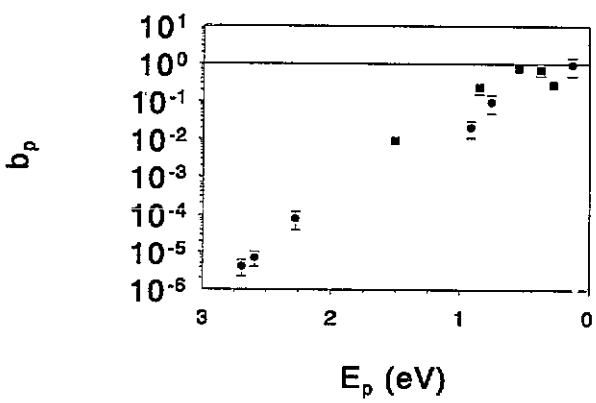

Figure 11. Population factors b_p for hydrogen and argon against E_p, the ionization energy of the level concerned ($z = 40$ mm, 3 vol.% hydrogen). Squares denote hydrogen levels, whereas circles represent argon levels.

broadening would be of any influence, the line profiles of higher excited levels would be broader. We can, thus, safely assume that all hydrogen Balmer line profiles are smaller than the apparatus profile (which equals 0.16 nm).

Another physical process must therefore be responsible for this bulge, and the most likely candidate is, once more, the occurrence of reactions (4) and (5), resulting in an extra input of hydrogen excited states. The fact that

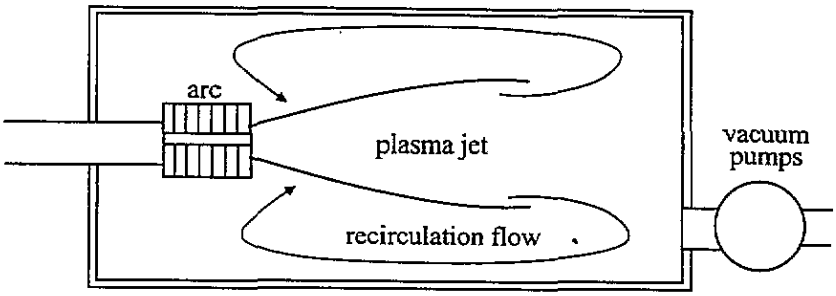

Figure 12. A sketch of the envisaged recirculation pattern in the vacuum vessel. This recirculation flow is thought to transport wall-associated hydrogen molecules towards the plasma, especially around the shock region.

the maximum of the bulge is not fixed, but can be found around $p = 5$–7 makes a excitation exchange process (e.g. between Ar (4p') and the H(I) system) unlikely, as this would be a very state-selective process. No evidence for excitation exchange processes between argon and hydrogen has been found using laser induced fluorescence experiments [22]. If vibrationally excited hydrogen molecules participate in reaction (4), however, the hydrogen produced in the dissociative recombination reaction (5) could appear in a highly excited state, thus explaining the bulge. The exact location of the maximum would then depend on the amount of vibrational (and rotational) excitation of the hydrogen molecules.

4. Conclusions

The transport phenomena of the expanding cascaded arc plasma remain unaffected for small hydrogen seed fractions: the neutral density behaviour is virtually unaffected by the addition of hydrogen and is well described by a quasi one-dimensional model, where the plasma parameters are averaged over a surface at right angles with the expansion axis.

The electron density is strongly affected by the addition of hydrogen: a strong decrease of the electron density is observed. This effect can be modelled using the quasi one-dimensional approximation, assuming that a certain number of hydrogen molecules form at the vessel walls and re-enter the plasma before and in the shock region. With this extra input from the periphery, a very good agreement between model and experiments is obtained.

A recirculation pattern within the vacuum vessel (figure 12) is thought to be responsible for the re-entry flow of hydrogen molecules into the jet. The largest fraction of these re-entering molecules must reach the beam before or in the shock region.

The electron temperature behaviour is reasonably well described by the model. However, since current generation has not been taken into account, the observed rise of the electron temperature before the actual shock position (equation [18]) cannot be modelled.

The behaviour of the cascaded arc itself changes dramatically when the hydrogen seed fraction exceeds 3 vol.%. This is shown by the fact that the electron density drops to levels below the detection limit of the Thomson–Rayleigh scattering set-up, even just outside the nozzle exit (for a 10 vol.% seed fraction).

The Ar(I) excited level population is determined by three-particle recombination: therefore the Ar(I) line intensities drop when hydrogen is added to the flow, resulting in a net loss of argon ions. The hydrogen excited level population arises due to three-particle recombination and dissociative recombination (equation (5)). The hydrogen Balmer emission decreases for higher seed fractions, most probably due to the reduced arc efficiency.

The 'bulge' in the hydrogen excited level distribution (b_p against E_p) can be attributed to the dissociative recombination of the ArH^+ molecular ion. If any rovibrational excitation of the hydrogen molecules is present, the formed hydrogen atom could end up in a highly excited state.

Acknowledgments

The authors gratefully acknowledge H M M de Jong, M J F van de Sande, and A B M Hüsken for their skillful technical assistance. This work is supported by the Netherlands Technological Foundation (STW). The work of M C M van de Sanden is supported by the Royal Netherlands Academy of Arts and Sciences (KNAW).

References

[1] Meulenbroeks R F G, van Beek A J, van Helvoort A J G, van de Sanden M C M and Schram D C 1994 *Phys. Rev.* E **49** (5) 4397

[2] de Graaf M J, Severens R, Dahiya R P, van de Sanden M C M and Schram D C 1993 *Phys. Rev.* E **48** (3) 2098

[3] van de Sanden M C M, de Regt J M, Janssen G M, van der Mullen J A M, Schram D C and van der Sijde B 1992 *Rev. Sci. Instrum* **63** (6) 3369

[4] Buuron A J M, Meeusen G J, Beulens J J, van de Sanden M C M and Schram D C 1993 *J. Nucl. Mater.* **200** 430

[5] Wilbers A T M, Meeusen G J, Haverlag M, Kroesen G M W and Schram D C 1991 *Thin Solid Films* **204** 59

[6] Meulenbroeks R F G, Schram D C, Jaegers L J M and van de Sanden M C M 1992 *Phys. Rev. Lett.* **69** (9) 1379

[7] Kroesen G M W, Schram D C, Wilbers A T M and Meeusen G J 1991 *Contrib. Plasma Phys.* **31** (1) 27
[8] van de Sanden M C M, van den Bercken R and Schram D C 1994 *Plasma Sources Sci. Technol.* **3** 511
[9] Gislason E A and Parlant G 1991 *J. Chem. Phys.* **94** (10) 6598
[10] van de Sanden M C M 1991 *PhD Thesis* Eindhoven University of Technology
[11] Braginskii S I 1965 *Reviews of Plasma Physics* ed M A Leontovich (New York: Plenum)
[12] Venugopalan H 1971 *Reactions under Plasma Conditions* (London: Wiley Interscience)
[13] Timmermans C J 1984 *PhD Thesis* Eindhoven University of Technology
[14] Kroesen G M W 1988 *PhD Thesis* Eindhoven University of Technology
[15] van de Sanden M C M, de Regt J M and Schram D C 1993 *Phys. Rev.* E **47** (4) 2792
[16] Ervin K M and Armentrout P B 1985 *J. Chem. Phys.* **83** (1) 166
[17] Mott-Smith H M 1951 *Phys. Rev.* **82** 885
[18] Muckenfuss C 1960 *Phys. Fluids* **3** 320
[19] Glansdorff P 1962 *Phys. Fluids* **5** 371
[20] Ashkenas H and Sherman F S 1966 *Rarefied Gas Dynamics* Vol **4** ed J H de Leeuw (New York: Academic)
[21] van der Mullen J A M 1989 *Phys. Rep.* **191** 109
[22] Engeln R A H, Meulenbroeks R F G, Snoeijer A J, van der Mullen J A M and Schram D C 1994 to be published
[23] Meeusen G J, Ershov-Pavlov E A, Meulenbroeks R F G, van de Sanden M C M and Schram D C 1992 *J. Appl. Phys.* **71** (9) 4156